TU Delft

Delft University of Technology

Copper promotion of chromium-doped iron oxide water-gas shift catalysts under industrially relevant conditions

Ariëns, M. I.; van de Water, L. G.A.; Dugulan, A. I.; Brück, E.; Hensen, E. J.M.

DOI
10.1016/j.jcat.2021.12.013

Publication date
2022

Document Version
Final published version

Published in
Journal of Catalysis

Citation (APA)
Ariëns, M. I., van de Water, L. G. A., Dugulan, A. I., Brück, E., & Hensen, E. J. M. (2022). Copper promotion of chromium-doped iron oxide water-gas shift catalysts under industrially relevant conditions. *Journal of Catalysis*, *405*, 391-403. https://doi.org/10.1016/j.jcat.2021.12.013

Important note
To cite this publication, please use the final published version (if applicable).
Please check the document version above.

Copyright
Other than for strictly personal use, it is not permitted to download, forward or distribute the text or part of it, without the consent of the author(s) and/or copyright holder(s), unless the work is under an open content license such as Creative Commons.

Takedown policy
Please contact us and provide details if you believe this document breaches copyrights.
We will remove access to the work immediately and investigate your claim.

This work is downloaded from Delft University of Technology.
For technical reasons the number of authors shown on this cover page is limited to a maximum of 10.

Journal of Catalysis 405 (2022) 391–403

Contents lists available at ScienceDirect

Journal of Catalysis

journal homepage: www.elsevier.com/locate/jcat

Copper promotion of chromium-doped iron oxide water-gas shift catalysts under industrially relevant conditions

M.I. Ariëns [a,b], L.G.A. van de Water [c], A.I. Dugulan [a], E. Brück [a], E.J.M. Hensen [b,*]

[a] Fundamental Aspects of Materials and Energy, Delft University of Technology, Mekelweg 15, 2629 JB Delft, The Netherlands
[b] Laboratory of Inorganic Materials and Catalysis, Department of Chemical Engineering and Chemistry, Eindhoven University of Technology, P.O. Box 513, 5600 MB Eindhoven, The Netherlands
[c] Johnson Matthey, PO Box 1, Belasis Avenue, Billingham, Cleveland TS23 1LB, UK

ARTICLE INFO

Article history:
Received 7 September 2021
Revised 6 December 2021
Accepted 13 December 2021
Available online 23 December 2021

Keywords:
Water–gas shift reaction
Iron oxide
Copper
Promotion
In situ characterization

ABSTRACT

Copper promotion of chromium-doped iron oxide prepared via co-precipitation for high-temperature water–gas shift (WGS) catalysis is investigated. Low-temperature Mössbauer spectra demonstrate that copper doping delays hematite (α-Fe_2O_3) formation in the fresh catalyst, favoring the formation of small crystallites of ferrihydrite ($Fe_5HO_8{\cdot}4\ H_2O$). Catalysts are treated under industrial WGS conditions at 360 °C (activity evaluation) and 450 °C (ageing) at 2 and 25 bar. Mössbauer spectra show that chromium is incorporated in octahedral sites of the active magnetite (Fe_3O_4) phase, resulting in a partially oxidized structure. Copper doping did not affect the bulk magnetite structure of the activated catalyst, which points to the presence of a separate copper phase. Near-ambient pressure XPS shows that copper is in the metallic state. XPS of discharged catalysts evidenced that reaction at elevated pressure resulted in the surface reduction of Fe^{3+} to Fe^{2+}. Copper promotion enhances CO conversion under high-temperature WGS conditions.

© 2021 The Author(s). Published by Elsevier Inc. This is an open access article under the CC BY license (http://creativecommons.org/licenses/by/4.0/).

1. Introduction

Hydrogen is widely used in the production of bulk chemicals such as ammonia [1,2]. The International Energy Agency (IEA) estimates the global annual (2018) hydrogen production at 70 million tonnes [3]. Approximately 80% of hydrogen is produced from natural gas reforming (1), which is typically combined with a water–gas shift (WGS) step (2) [1,4].

$CH_4 + H_2O \rightleftarrows CO + 3H_2$ ($\Delta H = 206$ kJ mol^{-1}) (1)

$CO + H_2O \rightleftarrows H_2 + CO_2$ ($\Delta H = -40.6$ kJ mol^{-1}) (2)

In industry, the WGS reaction is usually performed in two stages [4–9]. High-temperature WGS (high-temperature shift, HTS) is typically performed at 350–450 °C using iron-oxide based catalysts. To achieve high CO conversion of this equilibrium-limited reaction, a second low-temperature step is included. This low-temperature shift (LTS) step is typically performed in the range of 190–250 °C using copper-based catalysts. In this configuration, the bulk of CO is removed during HTS with exit CO concentrations typically around 2–4% CO, while the residual CO is removed by LTS lowering the final CO concentration to 0.1–0.3% [5].

Magnetite, the active phase of the iron-based HTS catalyst, is formed *in situ* via partial reduction of the hematite precursor [6,10]. The dominant mechanism for the HTS reaction is of a regenerative redox type [11], involving a Fe^{2+}/Fe^{3+} redox couple which occupies octahedral sites in the bulk and at the surface of the inverse spinel structure of magnetite [12,13]. In industrial catalysts, magnetite is promoted by chromium and copper to enhance CO conversion [1,2]. Chromium is added for structural stabilization of the catalyst, which forms upon activation a solid solution with magnetite. Chromium is known to incorporate into octahedral sites of magnetite. Robbins *et al.* showed that chromium is incorporated into the octahedral sites of magnetite prepared by heating a mixture of Fe_2O_3 and Cr_2O_3 to 1100 °C in a CO/CO_2 mixture, chromium replacing an equal amount of Fe^{2+} and Fe^{3+} [14,15]. Topsøe and Boudart confirmed that chromium incorporates into the octahedral sites of magnetite after treatment of chromium doped hematite structures under HTS conditions [16]. The authors suggested that replacement of equal amounts of Fe^{2+} and Fe^{3+} in octahedral sites, as indicated by Robbins *et al.*, is unlikely. We recently confirmed that chromium incorporation occurs in the octahedral sites of magnetite, and showed that its presence results in a partially oxidized structure ($Fe_{3-x(1-\delta)}Cr_xO_4$) [32]. While earlier chemical promotion by chromium via the Cr^{3+}/Cr^{6+} redox couple has also been postulated [2,17], a recent study has clearly demonstrated that the

* Corresponding author.
E-mail address: e.j.m.hensen@tue.nl (E.J.M. Hensen).

https://doi.org/10.1016/j.jcat.2021.12.013
0021-9517/© 2021 The Author(s). Published by Elsevier Inc.
This is an open access article under the CC BY license (http://creativecommons.org/licenses/by/4.0/).

Cr^{3+}/Cr^{6+} redox couple is not operative during WGS [18]. Copper acts as a chemical promoter and exists as Cu^{2+} in the fresh catalyst. Upon activation in a CO/H_2O mixture Cu^{2+} segregates from the bulk to form Cu^0 nanoparticles [6]. The presence of metallic copper on activated catalysts was observed by several authors [19,20] both in H_2O/CO mixtures and under HTS conditions at ambient pressure. Zhu *et al.* showed that 30% of the Cu^0 surface is covered by an iron oxide layer due to strong metal-support interactions [6]. The iron oxide layer stabilizes Cu^0 nanoparticles against aggregation and provides new active sites that facilitate CO adsorption and H_2O dissociation [21]. Recently, Zhu *et al.* discovered that Cu^0 nanoparticles are prone to deactivation via sintering in accelerated ageing tests at 600 °C under reverse WGS conditions [22].

Tightening regulations on the use of Cr^{6+} [23] have led to exploration of alternative dopants to stabilise iron-based HTS catalysts [2,18]. A rational design approach to achieve this goal is hampered by a lack of understanding of the exact role of chromium and copper dopants under industrially relevant conditions. An important limitation of previous works is that catalysts are typically not investigated after use under industrially relevant HTS conditions, for which three aspects are relevant. First, activity evaluation should involve gas mixtures containing H_2, CO, CO_2, and H_2O, representative of gas compositions used in an industrial plant [5]. Second, stability should be evaluated using dedicated accelerated testing protocols, because WGS catalysts typically operate for 3–5 years [5]. Third, catalyst testing should include the use of elevated pressure, as HTS is typically performed at pressures up to 80 bar in an industrial plant [5].

The physico-chemical and catalytic properties of WGS catalysts are strongly determined by the preparation procedure [24]. Popa *et al.* compared the long term stability of iron-chromium-copper catalysts prepared via ammonia-assisted co-precipitation of iron and chromium nitrates followed by copper impregnation to catalysts prepared by a single NaOH co-precipitation step [25]. A separate impregnation step is usually used for loading copper, because copper forms water-soluble complexes with ammonia [25,26]. Catalysts prepared by co-precipitation/impregnation exhibited more than two times higher initial reaction rates than catalysts prepared via a single-step NaOH-assisted co-precipitation. However, after 100 h at 400 °C and 16 h at 500 °C in a H_2O/CO mixture at atmospheric pressure, the activity of the initially more active ammonia-precipitated catalyst was substantially lower than that of the NaOH-precipitated catalyst. Enhanced deactivation was explained by stronger copper sintering in the catalyst prepared by ammonia-assisted preparation, which contained a larger amount of copper nanoparticles at the surface [25]. Meshkani and Rezaei showed that NaOH-assisted co-precipitation of iron, chromium, and copper nitrates provided catalysts stable up to 20 h at 400 °C under HTS conditions at atmospheric pressure [24]. Catalysts aged at pH 10 at 60 °C and calcined at 400 °C provided the highest CO conversion. Single-step NaOH-assisted co-precipitation is therefore regarded as a suitable method to obtain stable WGS catalysts.

Despite many studies [6,22,24,27,28], there are only few investigations involving characterization of copper-chromium-doped iron-oxide-based HTS catalysts that were not exposed to air after prolonged activity evaluation under industrially relevant conditions, i.e., elevated pressure, relevant gas compositions, and prolonged exposure times [20]. Mössbauer spectroscopy is a powerful technique to study iron-based catalysts [29], including the incorporation of dopants in the active iron oxide phase [30]. Mössbauer spectra can be deconvoluted into contributions of different iron species present in complex structures such as those present in tetrahedral and octahedral sites of magnetite [31]. This allows for detailed investigation of local dopant incorporation and its impact on the Fe^{2+}/Fe^{3+} redox couple. Mössbauer spectroscopy has not been applied to investigate copper-doped HTS catalysts aged under close-to-industrial conditions. Incorporation of Cr^{3+} into the active Fe_3O_4 phase as studied using Mössbauer spectroscopy has been reported previously by us [32]. In the present study, we report on the promoting effect of copper in chromium-doped iron-oxide based HTS catalysts. Copper promotion at different dopant levels was investigated on catalysts treated for 96 h under industrially relevant HTS conditions at 2 bar and 25 bar. The bulk catalyst was investigated by Mössbauer spectroscopy and XRD, while the surface was analysed by XPS. Near-ambient pressure (NAP)-XPS was performed to investigate the copper dopant in a working catalyst.

2. Experimental

2.1. Catalyst preparation

Catalysts were prepared via a co-precipitation/calcination procedure described elsewhere [24]. Briefly, appropriate amounts of iron, chromium, and copper nitrates were dissolved in deionised water at 60 °C under vigorous stirring. The pH was subsequently raised to pH 10 by the addition of a NaOH solution and the resulting slurry was aged at 60 °C for 1 h. After filtration and washing, the precipitates were dried at 150 °C for 3 h and calcined in static air at 400 °C for 4 h. Target compositions of × = 0, 1, 3, and 5 wt% CuO in α-Fe_2O_3/Cr_2O_3/CuO (92-x/8/x) wt. % were chosen to investigate the influence of copper doping. A reference 100% α-Fe_2O_3 catalyst was synthesised to differentiate between the influence of chromium and copper doping. Some aspects of the calcined reference α-Fe_2O_3 and CrCu(0) catalysts have been published elsewhere [32].

2.2. Characterization

X-ray powder diffraction (XRD) patterns were recorded on a PANalitical X'pert pro diffractometer equipped with a PW3064 spinner between 10° < 2θ < 100°, step size 0.008°, using Cu-K_α radiation. Spectral fitting was performed with the HighScore Plus software. Crystallite sizes were calculated with the Scherrer equation. XRD measurements of used catalyst samples were performed under an argon atmosphere and special care was taken to not expose the used catalyst samples to air.

Transmission **^{57}Fe Mössbauer spectroscopy** was performed with constant-acceleration or sinusoidal velocity spectrometers using a ^{57}Co(Rh) source. Velocity calibration is reported relative to α-Fe at room temperature. The source and the absorbing samples were kept at the same temperature during measurements. Spectra were fitted using the Mosswinn 4.0 program [33]. Used catalyst samples were kept under argon before and during measurement.

Nitrogen physisorption was performed on a Micromeritics 2420 ASAP instrument. Samples were outgassed prior to analysis with nitrogen at 140 °C for at least 1 h.

Transmission electron microscopy (TEM) images were acquired on a FEI Tecnai 20 (type Sphera) transmission electron microscope. Samples were suspended in a small quantity of acetone by sonication, followed by dispersion over a Cu grid containing holey carbon film. Particle size distributions were obtained by counting 200 particles per sample.

X-ray photoelectron spectroscopy (XPS) measurements were performed on a Thermo Scientific K-Alpha spectrometer using an aluminium anode (Al Kα = 1486.6 eV). The pressure in the measurement chamber was $2*10^{-8}$ mbar. Binding energy calibration was performed relative to adventitious carbon at BE = 285 eV. Spectral fitting was performed using CasaXPS software (version

2.3.19PR1.0). The samples were suspended on carbon tape and transferred to the spectrometer under vacuum. Fe 3p regions were fitted by a method adapted from Yamashita and Hayes [34]. For the Fe^{3+} component, a linear background was used and a A(0.23,1,0)GL (10) line shape. The Fe 3p peak position was fixed between 55.9 and 56.1 eV, FWHM = 2.0 – 2.2 eV. These values are based on the fitting of a freshly calcined 8% Cr-doped catalyst with all iron present as Fe^{3+}. For the Fe^{2+} component, a linear background was used and a A(0.23,1,0)GL(10) line shape. The peak position was not fixed, FWHM = 2.0 – 2.2 eV.

Near-ambient-pressure X-ray photoelectron spectroscopy (NAP-XPS) measurements were performed on a lab-based SPECS system using Al Kα irradiation (1486.6 eV). A thorough description of the machine is provided elsewhere [35]. Spectra were recorded in a reaction cell positioned in the ultra-high vacuum chamber. CO gas was added via a mass flow controller, steam was added via a piezo valve. Experiments were performed at 0.76 mbar and pressure was controlled via a backpressure controller. Binding energy calibration was performed relative to lattice oxygen at BE = 529.7 eV.

2.2.1. Catalytic activity measurements

Catalytic performance in the WGS reaction was determined in a parallel micro-reactor setup. In a typical test, 6 reactor tubes were charged with calcined catalyst and diluted with α-Al_2O_3. The reactors were purged with nitrogen and the temperature was raised to 250 °C at a rate of 2 °C min^{-1}. Steam was added via a HPLC pump after which dry reaction gas (55% H_2, 14% CO, 6% CO_2, and 25 % N_2) was introduced to reach the desired composition (37% H_2, 9% CO, 4% CO_2, 17 % N_2, 33% H_2O). The temperature was then ramped to 450 °C at a rate of 1 °C min^{-1} and maintained for 24 h to activate and age the catalysts. After initial ageing the temperature was lowered to 360 °C and activity was measured for 24 h. This was followed by an additional ageing step at 450 °C and activity measurement at 360 °C, each step for 24 h. Effluent products were analysed using a continuous gas analyser to allow calculation of CO conversion. After the reaction sequence was completed, the temperature was lowered to 250 °C and the H_2, CO, and CO_2 flows were switched to N_2. When no more CO was observed in the exit stream the steam addition was switched off and the catalysts were allowed to cool to room temperature in nitrogen flow. Samples were kept under a nitrogen atmosphere after the reaction before being stored in a glovebox under argon atmosphere prior to characterization.

Some aspects of the used reference α-Fe_2O_3 and CrCu(0) catalysts have been published before [32].

3. Results and discussion

3.1. Calcined catalysts

Chromium-copper co-doped iron oxide catalysts were prepared via a method adapted from Meshkani and Rezaei [24]. Prior to characterisation, catalysts were dried at 150 °C followed by calcination at 400 °C in static air. The physico-chemical properties of the freshly calcined catalysts are shown in Table 1 and the corresponding XRD patterns in Fig. 1. All XRD reflections observed are consistent with the presence of hematite, irrespective of the dopant level. Formation of hematite is typical for (doped) iron oxide catalysts prepared via precipitation-calcination. Zhu *et. al.* [6] and Reddy *et al.* [36] mentioned the formation of hematite after calcination of similar materials. We observed that the position of the (1 1 0) reflection shifts to higher 2θ values for the chromium-doped samples in comparison to the α-Fe_2O_3 reference (Fig. 1). This shift is caused by a contraction of the unit cell, pointing to the incorporation of chromium with a smaller ionic radius (Cr^{3+}, 62 pm) than the cations in the host structure (Fe^{3+}, 65 pm) [37]. No significant shift in 2θ values was observed upon copper doping.

Considerable line broadening was observed in the XRD patterns of the CrCu(1–5) samples compared to CrCu(0) and the α-Fe_2O_3(ref) sample. The line broadening in the XRD patterns confirms the formation of small crystallites. It should be noted that the absence of reflections due to other phases does not exclude the presence of small (<3–4 nm) or amorphous oxides of iron, chromium, or copper [37].

Mössbauer spectroscopy was used to investigate in more detail the iron oxide phases in the calcined catalysts, including the possible formation of particles with a size smaller than a few nm not visible by XRD characterisation. Room-temperature Mössbauer spectra showed the presence of a magnetically split hematite phase [38,39] with a quadrupole splitting (QS) of −0.21 mm s^{-1} and an average hyperfine magnetic field between 50.5 T and 48.4 T in α-Fe_2O_3, CrCu(0), and CrCu(1) (Fig. 2, Table 2). The superparamagnetic (SPM) doublet with an isomer shift (IS) of 0.37 mm s^{-1}, which is observed for all the CrCu(1–5) catalysts, indicates the presence of bulk iron oxide species with high spin Fe^{3+} in octahedral positions [29]. In Mössbauer spectra measured at −269 °C (Fig. 2), magnetic splitting was regained and two sextets were observed for the CrCu(1–5) catalysts, while only one sextet was observed for the α-Fe_2O_3(ref) and CrCu(0) catalysts. The sextets with QS = -0.21 mm s^{-1} (Table 2), prevalent for all catalysts irrespective of the dopant level, confirm the presence of hematite [40]. In the Mössbauer spectrum of α-Fe_2O_3(ref), a QS of 0.40 mm s^{-1} was observed, which indicates that hematite underwent the Morin transition [38]. The Morin transition is a magnetic phase transition inherent to non-doped hematite, which typically occurs between −12 °C and −32 °C characterised by spin canting around the c-axis [39]. In Mössbauer spectra of CrCu(1–5), two sextets were observed indicating the presence of a second phase besides hematite. IS values of 0.37 mm s^{-1} and QS = -0.04 mm s^{-1} and a hyperfine magnetic field between 48 T and 49 T point to the presence of the 6-line ferrihydrite (Fe_5HO_8·4 H_2O) phase [41]. This shows that the SPM phase observed in the room-temperature Mössbauer spectra contains hematite as well as small particles of ferrihydrite. Copper doping led to a decreased spectral contribution of hematite from 100% in the copper-free catalysts to 22% in CrCu(1) (Table 2). The hematite fraction further decreased from 22% to 9% with increasing Cu content going from CrCu(1) to CrCu (5), which shows that copper has an inhibiting effect on hematite formation during calcination. This inhibiting effect indicates that copper is incorporated in the bulk ferrihydrite structure. The incorporation of Cu^{2+} ions into a solid solution of the Fe-Cr-Cu mixed-oxide catalyst precursor during calcination was confirmed in a recent high-resolution XANES study [42]. XRD analysis was not able to provide solid evidence for this due to the absence of ferrihydrite reflections in the XRD patterns, resulting from the small size of the Fe_5HO_8·4 H_2O crystallites.

3.2. Catalytic activity testing

The catalytic performance of the obtained samples was evaluated in a plug-flow reactor under industrially relevant HTS conditions (37% H_2, 9% CO, 4% CO_2, 17 % N_2, 33% H_2O). The tests were conducted at 2 and 25 bar to investigate the promotional effect of copper doping on CO conversion at near ambient (2 bar) as well as an industrially relevant pressure (25 bar). Freshly calcined catalysts were initially aged under HTS conditions at 450 °C for 24 h followed by activity measurements for 24 h at 360 °C (Fig. 3). The catalysts were then further aged for 24 h at 450 °C followed by activity measurement for 24 h at 360 °C.

Table 1
Physico-chemical properties of calcined catalysts.

Catalyst	d (nm)[a]	BET SA (m^2g^{-1})[c]	V_{tot} (cm^3g^{-1})	Average pore size (nm)	CuO (wt. %)[b]	Cr_2O_3 (wt. %)[b]
α-Fe_2O_3(ref)	44	45	0.22	19.9	0.0	0.0
CrCu(0)	25	110	0.25	9.2	0.0	7.5
CrCu(1)	*	135	0.21	6.3	1.0	8.5
CrCu(3)	*	132	0.20	6.0	3.1	8.4
CrCu(5)	*	157	0.23	5.9	5.1	8.4

[a]Based on the Scherrer equation from the FWHM of the α-Fe_2O_3 (1 1 0) reflection. Patterns of too low quality for fitting marked with an asterisk.
[b]Obtained by XRF analysis. Intended Cr_2O_3 and CuO concentrations differ slightly in some samples due to residual Na_2O (0.6–1.5 wt%) [25,26].
[c]Surface area, pore volume, and pore diameter were determined by applying the Brunauer-Emmett-Teller (BET) method to N_2 adsorption isotherms.

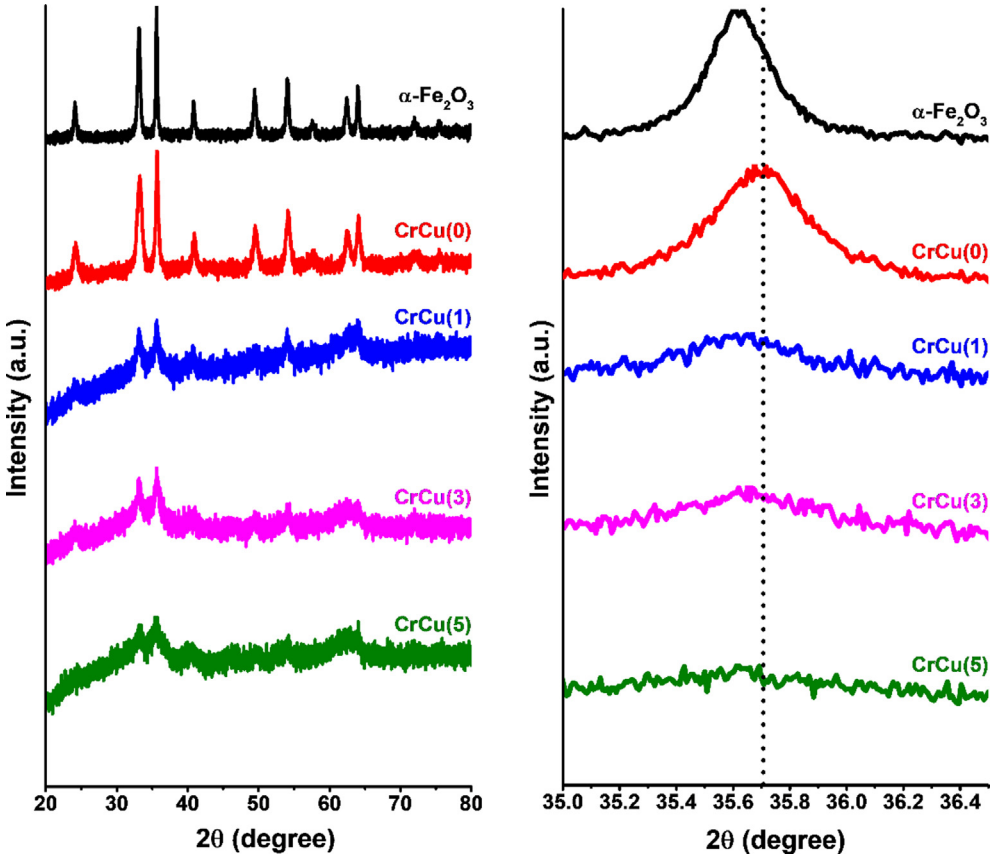

Fig. 1. XRD patterns of freshly calcined catalysts. Complete patterns (left). Patterns zoomed in on (1 1 0) reflection (right).

CO conversion levels during activity measurements at 2 bar are shown in Fig. 3. Higher CO conversion was observed after initial ageing of the CrCu(0) catalyst compared to the non-doped Fe_3O_4 catalyst. The better performance of the chromium-doped catalyst is usually explained by less extensive sintering of high-surface-area iron-based HTS catalysts [1,2]. Copper doping increased the CO conversion compared to CrCu(0). The increase in CO conversion was most pronounced for the CrCu(5) catalyst. The promoting effect of copper is typically attributed to the formation of Cu^0 nanoparticles on the surface of the bulk chromium-doped magnetite catalyst [6,21,22]. Cu^0 particles partially covered by an iron oxide over-layer can facilitate water dissociation, resulting in sites that are more active than individual copper and iron oxide sites [21]. The activity of CrCu(5) decreased after the second thermal ageing step.

The catalysts were also evaluated for their HTS performance at 25 bar. These experiments confirmed that copper doping led to a higher CO conversion after initial ageing compared to CrCu(0) and α-Fe_2O_3(ref) (referred to as Fe_3O_4 from this point) (Fig. 3). Thus, the promoting effect of copper is not strongly dependent on the pressure. We also observed that the second ageing step did not affect the CO conversion of the CrCu(0) catalyst (Fig. 3). The positive effect of copper on the CO conversion decreased and CO conversion levels were similar to that of the CrCu(0) sample. Deactivation of the copper doped catalysts can be the result of sintering of the Cu^0 nanoparticles [22], resulting in fewer active sites.

Used catalyst

The surface and bulk structure of the used catalysts was investigated by XRD, Mössbauer spectroscopy and XPS. XRD patterns of catalysts treated at 25 bar contain 2θ reflections at 29.9°, 35.3°, 42.9°, 53.3°, 56.8°, 62.4°, 70.8°, 73.9°, 86.6°, 89.5°, and 94.4° (Fig. 4), which point to the presence of either magnetite (Fe_3O_4) or maghemite (γ-Fe_2O_3) [43]. Since magnetite and maghemite possess a similar inverse spinel structure, no distinction can be made by XRD analysis alone [44]. No reflections due to copper- or chromium-containing phases were observed, which is in line with the expected size of the Cu^0 nanoparticles below a few nm [6] and the absence of separate chromium oxide phases.

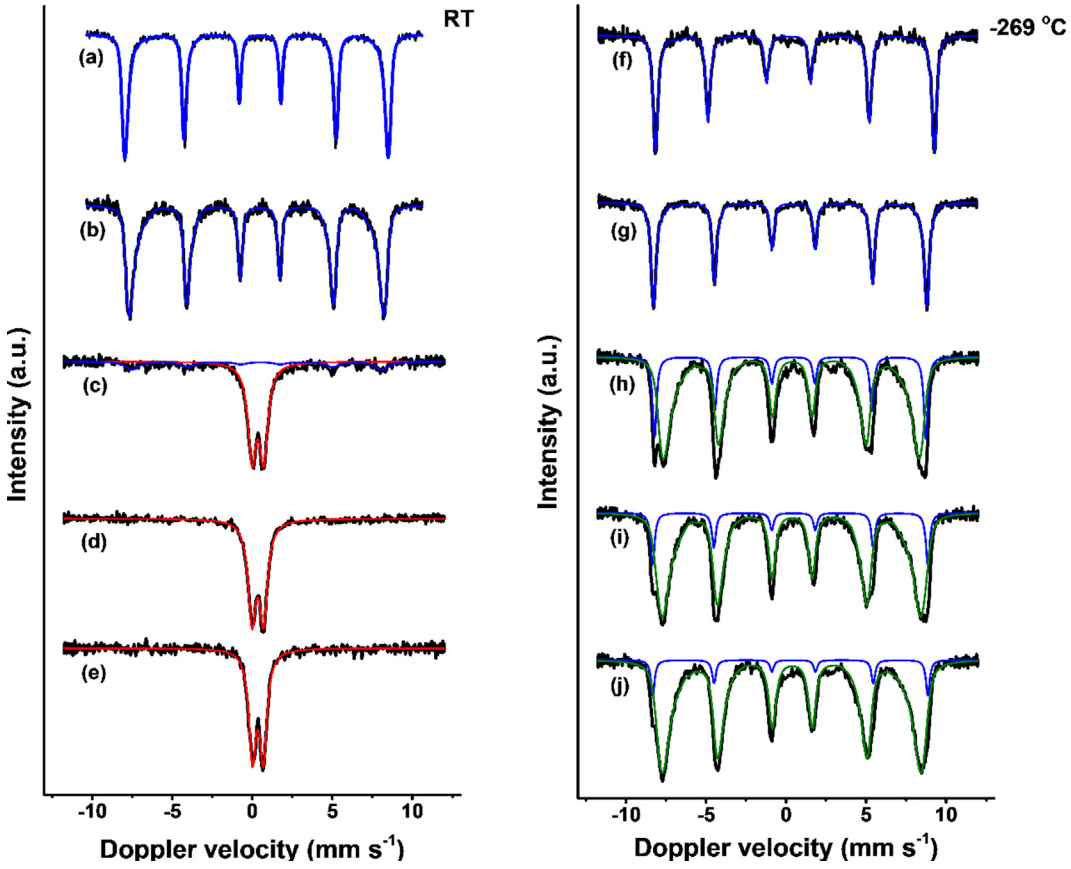

Fig. 2. Mössbauer spectra of freshly calcined catalysts. Room temperature Mössbauer spectra of: (a) α-Fe_2O_3(ref); (b) CrCu(0); (c) CrCu(1); (d) CrCu(3); (e) CrCu(5). Mössbauer spectra recorded at −269 °C of: (f) α-Fe_2O_3(ref); (g) CrCu(0); (h) CrCu(1); (i) CrCu(3); and (j) CrCu(5).

Table 2
Mössbauer data of freshly calcined catalysts obtained at room temperature and −269 °C.

T (°C)	Catalyst	IS (mm s^{-1})	QS (mm s^{-1})	Hyperfine field (T)	Γ (mm s^{-1})	Phase	Spectral contribution (%)
RT	α-Fe_2O_3 (ref)	0.38	−0.23	50.5†	0.23	α-Fe_2O_3	100
	CrCu(0)	0.38	−0.21	48.5†	0.25	α-Fe_2O_3	100
	CrCu(1)	0.35	0.72	–	0.62	Fe^{3+} SPM	78
		0.39	−0.24	48.4	0.98	α-Fe_2O_3	22
	CrCu(3)	0.34	0.71	–	0.59	Fe^{3+} SPM	100
	CrCu(5)	0.35	0.68	–	0.57	Fe^{3+} SPM	100
−269 °C	α-Fe_2O_3(ref)	0.35	0.40	53.6†	0.28	α-Fe_2O_3	100
	CrCu(0)	0.36	−0.21	52.7†	0.26	α-Fe_2O_3	100
	CrCu(1)	0.35	−0.20	52.7	0.30	α-Fe_2O_3	22
		0.36	−0.06	48.1	0.45	$Fe_5HO_8 \cdot 4\ H_2O$	78
	CrCu(3)	0.36	−0.21	53.4	0.29	α-Fe_2O_3	14
		0.36	−0.04	48.9	0.48	$Fe_5HO_8 \cdot 4\ H_2O$	86
	CrCu(5)	0.37	−0.21	53.4	0.27	α-Fe_2O_3	9
		0.37	−0.04	48.6	0.47	$Fe_5HO_8 \cdot 4\ H_2O$	91

[a]Fixed values are marked with an asterisk (*), average values of distribution fits with a dagger (†).
[b]Experimental uncertainties: IS ± 0.01 mm s^{-1}, QS ± 0.01 mm s^{-1}, line width: Γ ± 0.01 mm s^{-1}, hyperfine magnetic field: ± 0.1 T, spectral contribution: ± 3%.

Room-temperature Mössbauer spectra demonstrate that magnetite was formed during operation under HTS conditions (Fig. 5). Detailed information on local dopant incorporation, including their location in tetrahedral and octahedral sites, can be obtained by deconvoluting the Mössbauer spectra into subspectra representing the various sites [31,45]. IS and hyperfine magnetic field values of respectively ∼ 0.28 mm s^{-1} and ∼ 48.5 T were observed for the tetrahedral sites, irrespective of the presence of copper and chromium (Table 3). These values are similar with those reported by Reddy *et al.* [28] for used HTS catalysts under atmospheric conditions and show that dopants are not incorporated in tetrahedral sites. The IS value of the octahedral sites decreased from 0.68 mm s^{-1} for the non-doped Fe_3O_4 catalysts to 0.64 mm s^{-1} for the CrCu(0–5) samples (Table 3). This decrease from the bulk value of ∼ 0.67 mm s^{-1} points to partially oxidized octahedral sites upon chromium incorporation [32,44,46]. The higher than unity Fe^{3+}/Fe^{2+} ratio in the octahedral sites upon chromium doping can be the result of the octahedral site preference of Cr^{3+} which during magnetite formation hinders Fe^{3+} reduction [47]. Very similar IS values were observed for the CrCu(0), CrCu (1), CrCu(3) and CrCu(5) samples, indicating that copper has no effect on the average iron oxidation state in the octahedral sites

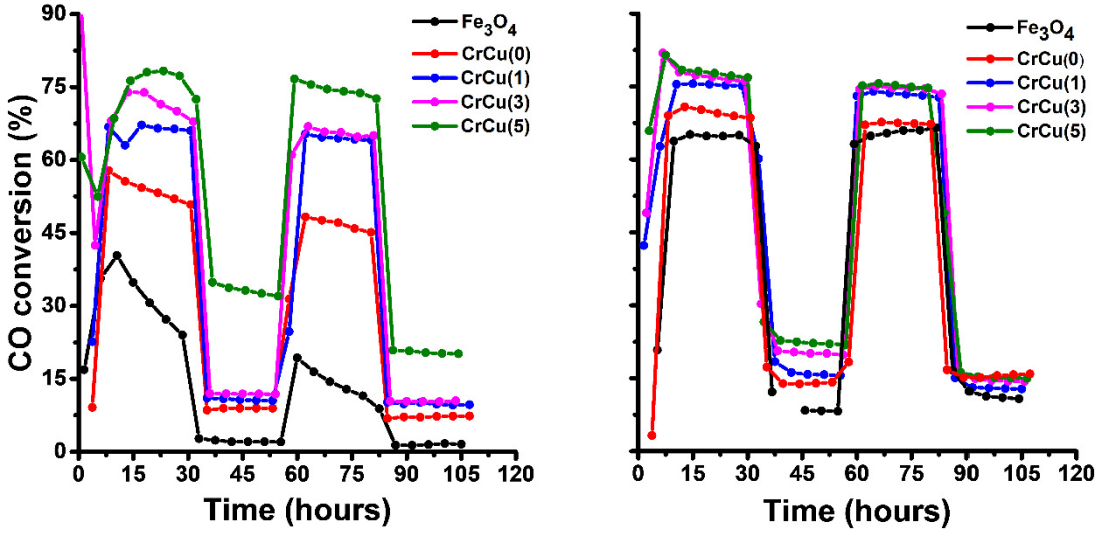

Fig. 3. CO conversion over time at 2 bar (left) and 25 bar (right). The α-Fe_2O_3 phase present in the α-Fe_2O_3(ref) catalyst is transformed into Fe_3O_4 during the reaction. CO conversion of the Fe_3O_4 and CrCu(0) reference catalysts at 25 bar were recorded in a separate run than the samples characterised in the next section.

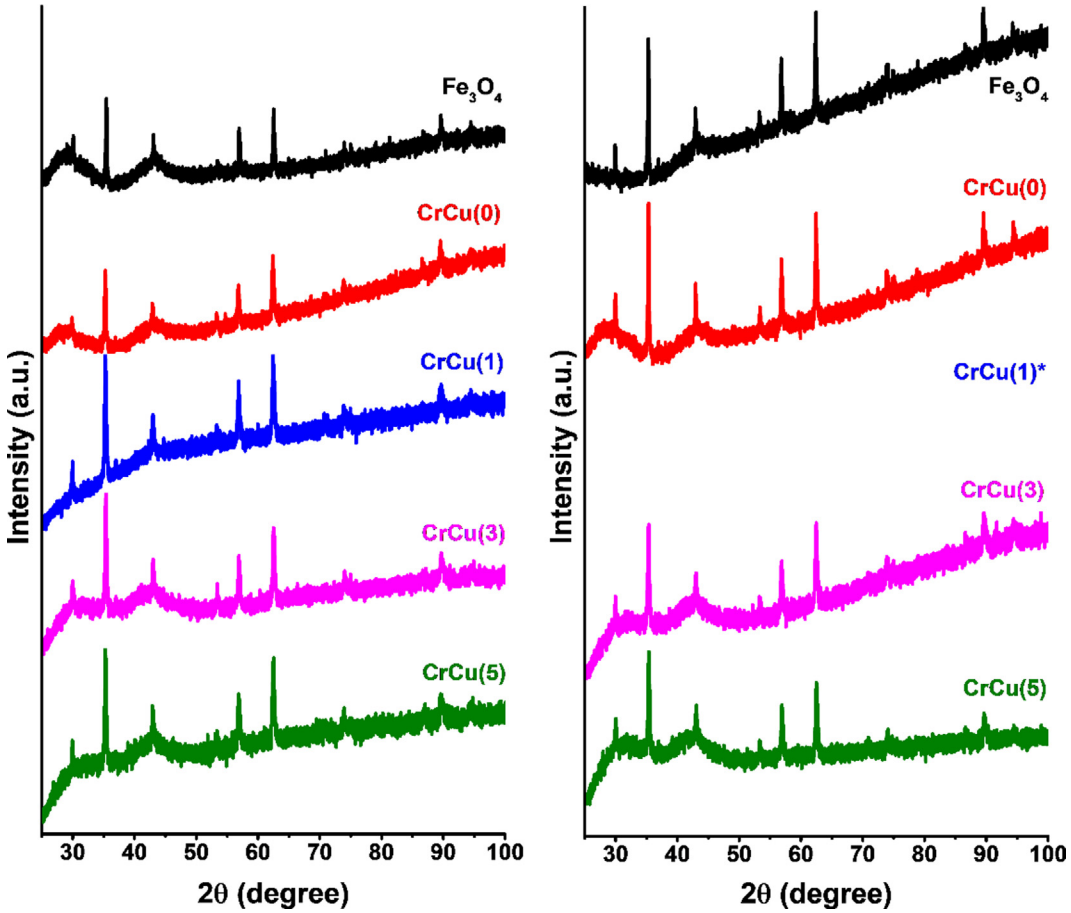

Fig. 4. XRD patterns after treatment under HTS conditions for 96 h at 2 bar (left) and 25 bar (right). *no XRD pattern for CrCu(1) after 25 bar was recorded.

in the activated catalysts. The similar IS values suggest that no copper is incorporated into the octahedral sites, since the incorporation of divalent ions like Cu^{2+} is expected to replace divalent Fe^{2+} ions resulting in a more Fe^{3+}-like IS in the octahedral sites. The absence of copper in octahedral sites contradicts an earlier Mössbauer study by Reddy *et al.* [28]. These authors based their conclusion that copper is incorporated into the octahedral sites of magnetite on a decrease in the ratio of the octahedral/tetrahedral site spectral contributions. A decreased ratio of the spectral contribution of the octahedral and tetrahedral sites can however also indicate the presence of a maghemite phase, which can form upon exposure of the active magnetite phase to air. The spectral contri-

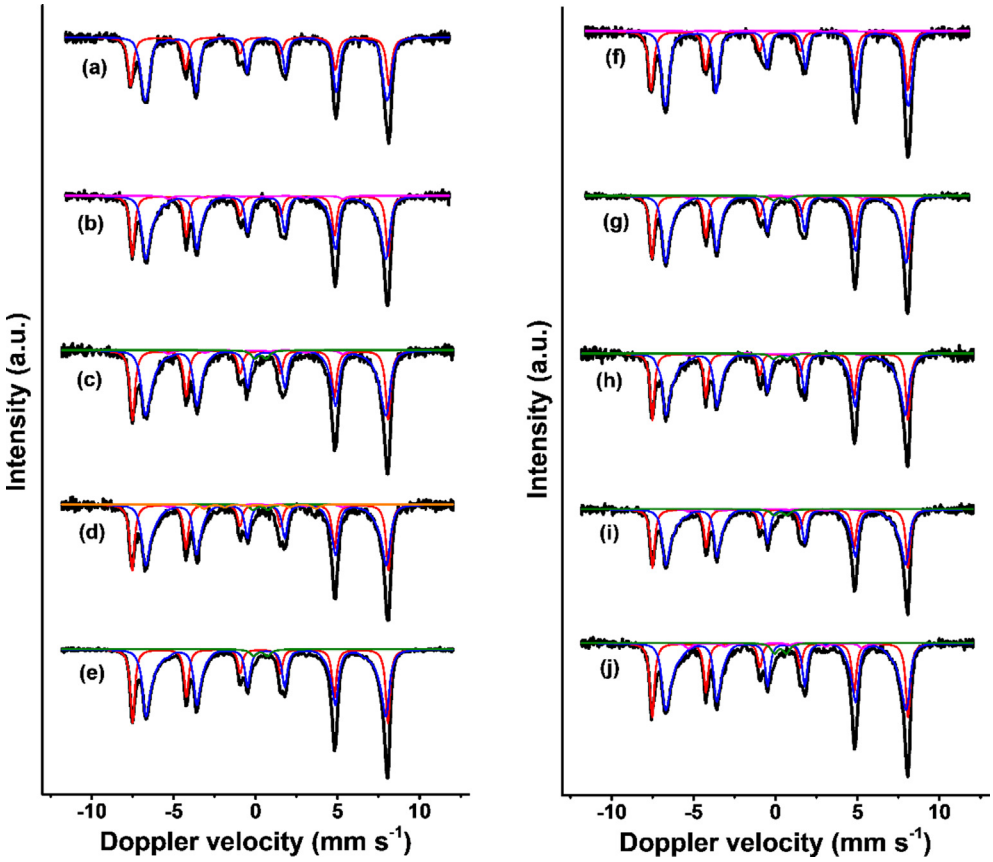

Fig. 5. Mössbauer spectra recorded at room temperature of catalysts treated under HTS conditions for 96 h at 2 bar: (a) α-Fe_2O_3(ref); (b) CrCu(0); (c) CrCu(1); (d) CrCu(3); (e) CrCu(5); and 25 bar: (f) α-Fe_2O_3(ref); (g) CrCu(0); (h) CrCu(1); (i) CrCu(3); (j) CrCu(5). Spectral contributions of the tetrahedral and octahedral sites of magnetite are shown in red and blue respectively. Minor spectral contributions indicating the presence of an α-Fe (magenta), and Fe_3C (orange) were observed, indicating some over-reduction of the active catalyst with no apparent trend with respect to the presence of dopants or pressure. The Fe^{3+} SPM phase (green) indicates the presence of a small particle magnetite phase. (For interpretation of the references to colour in this figure legend, the reader is referred to the web version of this article.)

Table 3
Mössbauer parameters of catalysts exposed to HTS conditions for 96 h at 25 bar.

Catalyst	IS (mm s^{-1})	QS (mm s^{-1})	Hyperfine field (T)	Γ (mm s^{-1})	Phase	Spectral contribution (%)
Fe_3O_4[a]	0.26	−0.03	48.7	0.38	Fe_3O_4(tet)	37
	0.68	−0.03	45.7†	0.32	Fe_3O_4(oct)	62
	0.00*	0.00*	33.0*	0.50*	α-Fe	1
CrCu(0)	0.28	0.00	48.6	0.34	Fe_3O_4(tet)	35
	0.64	−0.01	44.6†	0.32	Fe_3O_4(oct)	61
	0.00*	0.00*	33.0*	0.50*	α-Fe	2
	0.30*	0.86	-	0.50*	Fe^{3+} SPM	2
CrCu(1)	0.28	0.01	48.5	0.31	Fe_3O_4(tet)	33
	0.64	−0.02	44.1†	0.30	Fe_3O_4(oct)	63
	0.00*	0.00*	33.0*	0.50*	α-Fe	2
	0.30*	0.83	-	0.50*	Fe^{3+} SPM	2
CrCu(3)	0.29	0.00	48.4	0.32	Fe_3O_4(tet)	34
	0.64	−0.03	44.2†	0.30	Fe_3O_4(oct)	62
	0.00*	0.00*	33.0*	0.50*	α-Fe	2
	0.30*	0.76	-	0.50*	Fe^{3+} SPM	2
CrCu(5)	0.28	−0.00	48.5	0.33	Fe_3O_4(tet)	34
	0.65	−0.02	44.3†	0.30	Fe_3O_4(oct)	59
	0.00*	0.00*	33.0*	0.50*	α-Fe	4
	0.30*	0.73	-	0.50*	Fe^{3+} SPM	3

[a] Fe_3O_4 corresponds to activated α-Fe_2O_3(ref).
[b] Fixed values are marked with an asterisk (*), average values of distribution fits with a dagger (†).
[c] Experimental uncertainties: IS ± 0.01 mm s^{-1}, QS ± 0.01 mm s^{-1}, line width: Γ ± 0.01 mm s^{-1}, hyperfine magnetic field: ± 0.1 T, spectral contribution: ± 3%.

bution of maghemite overlaps with the tetrahedral site contribution of magnetite because of its similar hyperfine magnetic field. QS values of ∼ 0.00 mm s^{-1} were observed for both the tetrahedral and octahedral sites, which is typical for magnetite (Table. 3) [41]. The hyperfine magnetic field of the octahedral sites decreased from 45.7 T to ∼ 44.3 T for the chromium-doped catalysts (Table 3, Fig. 5). The deviation of the hyperfine magnetic field from the bulk value of 46.0 T confirms that chromium is incorporated in the octa-

hedral sites [48]. No significant decrease in hyperfine magnetic field values was observed for the samples that contained copper (Table 3, Fig. 5). Thus, copper does not remain included in the iron oxide phase and the decreased hyperfine magnetic field arises solely from chromium incorporation. Particle size effects on the hyperfine magnetic field values are unlikely, because the decrease only occurs for the octahedral sites. The Mössbauer parameters for the tetrahedral sites remain the same. These results point to the removal of Cu^{2+} from the bulk iron oxide structure upon activation of the catalyst [6]. The absence of copper in the bulk $Fe_{3-x(1-\delta)}Cr_xO_4$ phase after exposure to HTS conditions for 96 h at 25 bar is in line with the observation of a separate Cu^0 phase by Zhu *et al.* [6] and Zhu *et al.* [22], who tested their catalysts at ambient pressure in a H_2O/CO mixture and under reverse WGS conditions, respectively.

After treatment for 96 h at 2 bar, the XRD reflections are similar to those of catalysts treated at 25 bar (Fig. 4). Again, no reflections due to separate copper or chromium species were observed. Mössbauer spectra (Fig. 5, Table 4) showed the same decreased IS values from the bulk value to 0.64 mm s^{-1} in the CrCu(0–5) catalysts. For the Fe_3O_4 reference catalyst, an IS of 0.64 mm s^{-1} was observed. The unexpected decrease in IS, together with a hyperfine magnetic field of 49.0 T observed for the tetrahedral sites, points to accidental oxidation, resulting in the formation of a small amount of maghemite and partially oxidized magnetite. Since maghemite is known to transform into magnetite under WGS conditions [8], it is unlikely that this is the result of the process conditions. Incorporation of chromium in the octahedral sites of magnetite was confirmed by decreased hyperfine magnetic field values from the value of 45.6 T CrCu(0–5) samples compared to the reference Fe_3O_4 catalyst (Table 4). The catalysts treated at 2 bar also show no effect of copper on the hyperfine magnetic field, indicating that copper was not incorporated into the $Fe_{3-x(1-\delta)}Cr_xO_4$ structure, in good agreement with earlier observations [6,21,22]. These results show that the incorporation of chromium into the octahedral sites resulting in partial oxidation and the expulsion of copper from the bulk structure are independent of pressure.

Crystallite sizes of calcined α-Fe_2O_3 and used Fe_3O_4 catalysts obtained from XRD analysis are shown in Table 5. The average crystallite size of discharged catalysts after treatment at 2 bar is 71 nm for the non-doped Fe_3O_4 catalyst, which implies significant sintering compared to the average crystallite size of 44 nm of the fresh α-Fe_2O_3(ref) catalyst. The crystallite size of CrCu(0) increases from 25 nm in the fresh state to 41 nm after reaction at 2 bar for 96 h. The lower degree of sintering of CrCu(0) can be attributed to chromium doping, which is known to prevent thermal agglomeration [1,2]. Crystallite sizes of freshly calcined copper-doped samples could not be determined due to the broadness of XRD reflections caused by the presence of a ferrihydrite phase that is either amorphous or has very small crystallite size (Fig. 1). After treatment at 2 bar, average crystallite sizes of 39 nm in CrCu(1), 47 nm in CrCu(3), and 46 nm in CrCu(5) were observed. These crystallite sizes are similar to those of the CrCu(0) catalyst and lower than the crystallite sizes of the non-doped Fe_3O_4 reference catalyst. The lower crystallite size can be attributed to chromium incorporation, stabilizing the high surface area of the catalyst [1,2]. These results show that, while the presence of copper resulted in smaller crystallites of the calcined catalyst, copper did not affect the crystallite size during the HTS reaction. This provides further evidence of the expulsion of copper from the bulk structure in line with the promotion mechanism of a separate Cu^0 phase proposed by Zhu *et al.* [6]. Catalysts treated at 25 bar showed a similar trend in average crystallite sizes with the exception of CrCu(0) (Table 5). We believe that this is an outlier, because there has been no prior evidence for the role of Cu as a structural promoter. Furthermore, this effect is not observed for the catalysts aged at 2 bar. The decrease in crystallite size for the chromium-doped catalysts confirms that chromium acts as a structural stabilizer [1,2]. The similar crystallite sizes measured for the copper-doped samples together with

Table 5
Average crystallite sizes of spent catalysts after treatment under HTS conditions for 96 h as determined by XRD analysis.

	Fresh[a]	2 bar	25 bar
Fe_3O_4	44b	71b	74
CrCu(0)	25	41	64
CrCu(1)	*	39	n.m.
CrCu(3)	*	47	43
CrCu(5)	*	46	43

[a] Freshly calcined catalysts.
[b] Calculated with the Scherrer equation from the FWHM of the α-Fe_2O_3 (1 1 0) reflection and the Fe_3O_4 (3 1 1) reflection.

Table 4
Mössbauer parameters of catalysts exposed to HTS conditions for 96 h at 2 bar.

Catalyst	IS (mm s^{-1})	QS (mm s^{-1})	Hyperfine field (T)	Γ (mm s^{-1})	Phase	Spectral contribution (%)
$Fe_3O_4^{a,+}$	0.28	−0.04	49.0	0.38	Fe_3O_4(tet)	35
	0.64	−0.00	45.6†	0.29	Fe_3O_4(oct)	63
	0.00*	0.00*	33.0*	0.50*	α-Fe	2
CrCu(0)	0.29	−0.01	48.5	0.33	Fe_3O_4(tet)	33
	0.64	−0.02	44.3†	0.33	Fe_3O_4(oct)	64
	0.00*	0.00*	33.0*	0.50*	α-Fe	3
CrCu(1)	0.29	−0.00	48.5	0.37	Fe_3O_4(tet)	35
	0.64	−0.03	44.4†	0.36	Fe_3O_4(oct)	60
	0.00*	0.00*	33.0*	0.50*	α-Fe	2
	0.30*	0.70	-	0.50*	Fe^{3+} SPM	3
CrCu(3)	0.28	0.00	48.6	0.35	Fe_3O_4(tet)	35
	0.64	0.00	44.6†	0.35	Fe_3O_4(oct)	58
	0.00*	0.00*	33.0*	0.50*	α-Fe	2
	0.30*	0.91	-	0.50*	Fe^{3+} SPM	2
	0.19*	0.18	21.2*	0.50*	Fe_3C	3
CrCu(5)	0.29	−0.01	48.4	0.32	Fe_3O_4(tet)	35
	0.64	−0.01	44.3†	0.34	Fe_3O_4(oct)	63
	0.30*	0.86	-	0.50*	Fe^{3+} SPM	2

[a] Fe_3O_4 corresponds to activated α-Fe_2O_3(ref).
[b] Fixed values are marked with an asterisk (*), average values of distribution fits with a dagger (†).
[c] Experimental uncertainties: IS ± 0.01 mm s^{-1}, QS ± 0.01 mm s^{-1}, line width: Γ ± 0.01 mm s^{-1}, hyperfine magnetic field: ± 0.1 T, spectral contribution: ± 3%.
+ The decreased IS for the reference Fe_3O_4 catalyst is likely due to accidental oxidation.

increased CO conversion are in line with a chemical promotion mechanism.

TEM was used to explore the particle sizes of the various samples in more detail (Fig. 6). The average crystallite sizes of the copper-doped catalysts after treatment at 25 bar were very similar (i.e., 52 nm for CrCu(1), 50 nm for CrCu(3), and 48 nm for CrCu(5)), close to the values derived by XRD. The similar average crystallite sizes confirm that the promoting effect of copper doping is of a chemical nature.

XPS measurements were performed to investigate the surface structure of the used catalysts. The Fe 2p XPS spectra of catalysts treated at 2 bar and 25 bar are shown in Fig. 7. The typical satellite feature due to Fe^{3+} at a binding energy (BE) of 719 eV was absent for all samples, which is in line with the predominance of magnetite [6] as followed from Mössbauer spectroscopy and XRD. Surface Fe^{3+}/Fe^{2+} ratios were approximated by fitting the Fe 3p region (Fig. 8) according to the method proposed by Yamashita and Hayes [34]. A lower Fe^{3+}/Fe^{2+} ratio was observed for all catalysts treated at 25 bar compared to those treated at 2 bar. The exception is CrCu(5), which exhibited similar Fe^{3+}/Fe^{2+} ratios after the two experiments. The more ferrous-like surface of the catalyst after treatment at elevated pressure can be explained by the reducing nature of the gas mixture. In the Cr 2p region (Fig. 9), the peak at a BE of 577 eV indicates that chromium is present as Cr^{3+} [49], which is in line with observations by others [6].

Analysis of the Cu 2p region (Fig. 10) confirmed the presence of copper on the surface of the used catalysts after treatment at 2 and 25 bar. The sharp peak at BE = 933 eV corresponds to either Cu^0 or Cu^+ oxide [51]. Inspection of the Cu LMM region (Fig. 10) shows a peak at a kinetic energy (KE) ~ 916.7 eV, which is characteristic for Cu^+ [51,52]. The formation of Cu^+ instead of metallic copper contradicts earlier findings by others [6,21,22] and could be the result of the shutdown procedure after activity measurements or accidental exposure to air. After cooling to 250 °C, the CO, CO_2, and H_2 streams were switched to N_2 before water addition was stopped to prevent accidental over-reduction of the active $Fe_{3-x(1-\delta)}Cr_xO_4$ phase. Oxidation of Cu^0 to Cu^+ by water was observed before [53] and is therefore a likely cause.

To further investigate the oxidation state of copper on the catalyst surface, NAP-XPS measurements were performed. Fig. 11 shows the Cu $2p_{3/2}$ region and the Cu LMM region of CrCu(5) before and during exposure to a CO/H_2O mixture at a total pressure of 0.76 mbar. The Cu $2p_{3/2}$ region of the calcined catalyst shows a strong satellite peak at BE = ~941 eV, which points to the presence of Cu^{2+}. Upon exposure to an atmosphere of steam (0.46 mbar) and raising the temperature from room temperature to 250 °C, the satellite peak at BE = ~941 eV disappeared and a sharp peak at BE = 932.3 eV became visible, which is typical for reduced Cu species (Cu^0 and/or Cu^+). Thus, heating in a steam atmosphere led to the reduction of Cu^{2+}. The reduction of Cu^{2+} ($CuO \rightarrow Cu_2O + ½ O_2$) was observed before for CuO nanowires during heating between 155 °C and 244 °C under vacuum in *in-situ* TEM experiments [54]. The Cu LMM feature at KE = ~916.5 eV confirms the formation of Cu^+. No change in Cu oxidation states was observed upon the replacement of the H_2O atmosphere by a CO/H_2O mixture at 250 °C. When the temperature was raised to 450 °C, a peak at

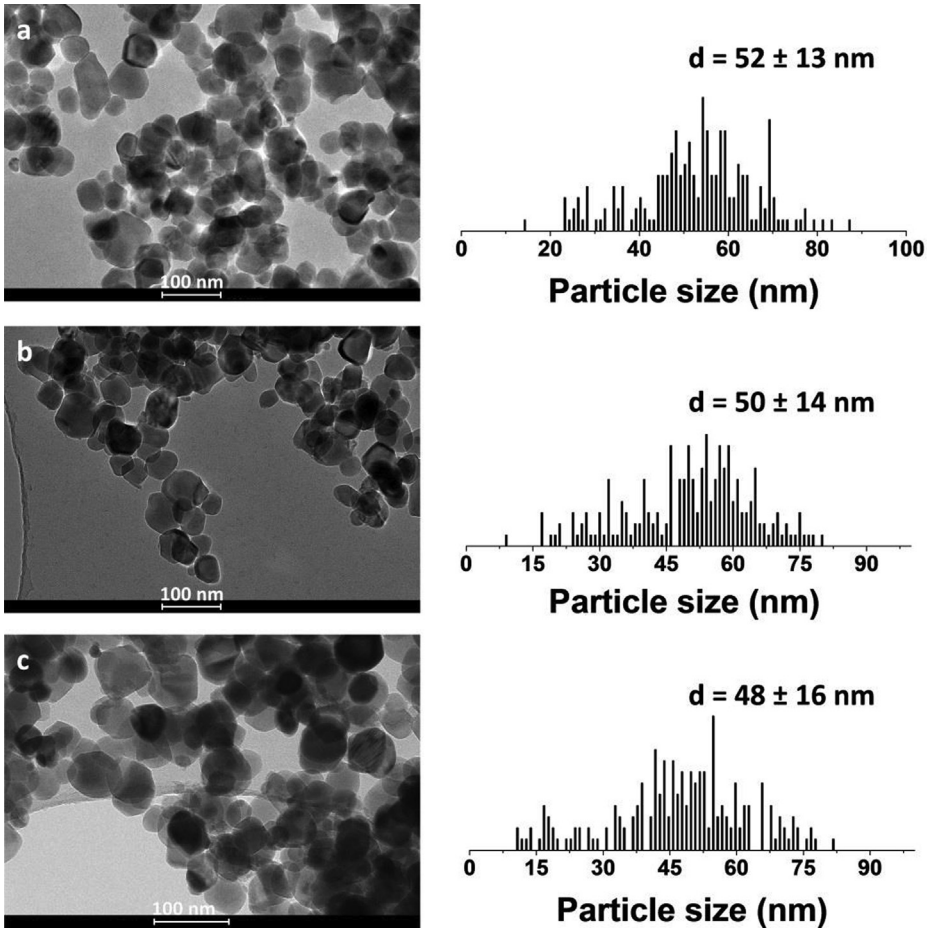

Fig. 6. TEM images and particle size distributions of discharged copper-doped catalysts after treatment under HTS conditions for 96 h at 25 bar: (a) CrCu(1); (b) CrCu(3); and (c) CrCu(5).

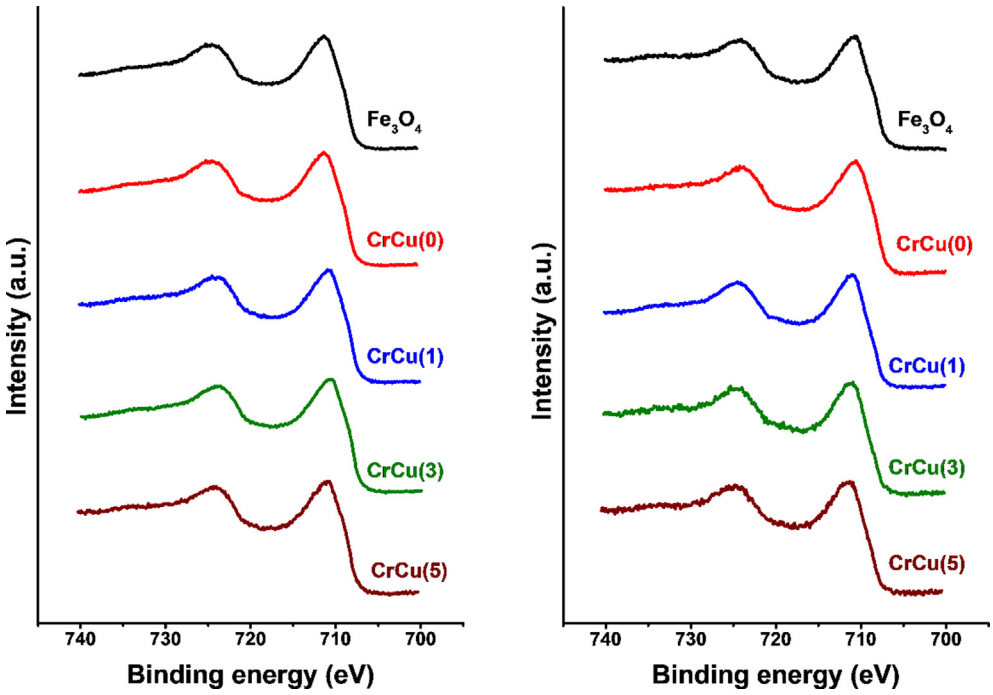

Fig. 7. Fe 2p region XPS spectra recorded after treatment of the catalysts under HTS conditions for 96 h at 2 bar (left) and 25 bar (right).

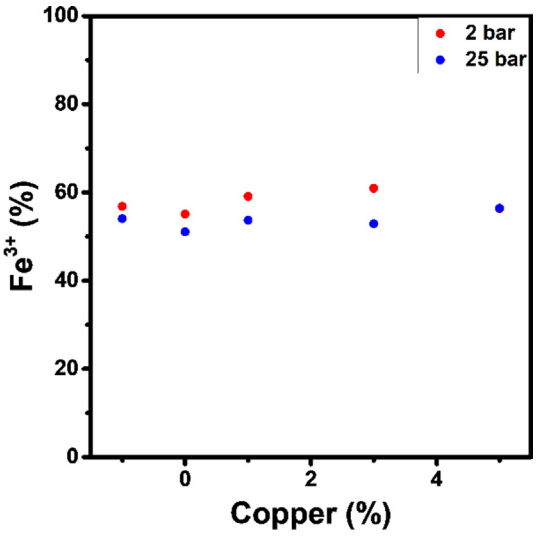

Fig. 8. Fe^{3+} content obtained from fitting Fe 3p region. The reference Fe_3O_4 value is shown at −1% on the x-axis. The fits are provided in the supporting info (Fig. S1).

KE = 918.8 eV was observed, while the peak at KE = 916.6 eV disappeared. This confirms the presence of metallic copper on the catalyst in a H_2O/CO mixture at 450 °C [6,21,22]. The temperature was then lowered to 250 °C and the catalyst was exposed to steam (0.46 mbar) at 250 °C overnight to mimic water exposure during the shutdown procedure of experiments as discussed above. Exposure to H_2O did not lead to the oxidation of Cu^0 to Cu^+. This is most likely the result of the low H_2O pressure during the NAP-XPS measurements (0.46 mbar) compared to 8.25 bar H_2O during the reactor activity evaluation at 25 bar. Exposure of the used catalyst to 0.3 mbar O_2 after cooling to RT in UHV also did not oxidize the catalyst, which further confirms that oxidation is hindered by low concentrations of the oxidizing gases. The NAP-XPS experiments confirm that copper is present as Cu^0 after exposure to a CO/H_2O mixture at 450 °C [6]. These experiments reveal that investigating HTS catalysts under NAP-XPS conditions is of limited value in understanding the dynamic phenomena occurring under industrially relevant HTS conditions and confirms the necessity to study carefully discharged catalysts used under relevant conditions. The presence of Cu^+ on the surface of the catalysts discharged after exposure to industrially relevant HTS conditions (Fig. 10) suggests that the oxidation of Cu^0 nanoparticles by H_2O on the active catalyst can easily occur under steam concentrations close to industrially relevant HTS conditions. This confirms that copper facilitates H_2O dissociation under industrially relevant conditions [21].

4. Conclusions

Hematite is the dominant phase in freshly calcined iron-oxide and chromium-doped iron-oxide WGS catalysts. Calcined chromium-iron-oxide catalysts doped with copper consist of a mixture of hematite and ferrihydrite. Mössbauer spectra of copper-containing samples show that copper inhibits the formation of hematite during calcination. The amount of ferrihydrite increases with the copper content. Hematite and small particles of ferrihydrite convert completely to magnetite under industrially relevant HTS gas compositions at 2 and 25 bar. Mössbauer spectra show that chromium forms a solid solution with magnetite by occupying octahedral sites, resulting in a partially oxidized Fe^{2+}/Fe^{3+} redox couple, which is known to be present in the bulk and at the surface of the catalyst. There was no effect of the pressure on the bulk structure. Copper doping had no significant effect on the hyperfine parameters in Mössbauer spectra, meaning that it is not likely that copper is incorporated in the bulk structure. NAP-XPS experiments confirmed copper exists as metallic copper at the catalyst surface under WGS conditions. Catalysts exposed to HTS conditions at 25 bar had a more ferrous like surface than catalysts treated at 2 bar due to the more reducing nature of the gas mixture at elevated pressure. Chromium stabilizes the high surface area of the catalyst at ambient and industrially relevant pressure, leading to a higher CO conversion. Copper promotes CO

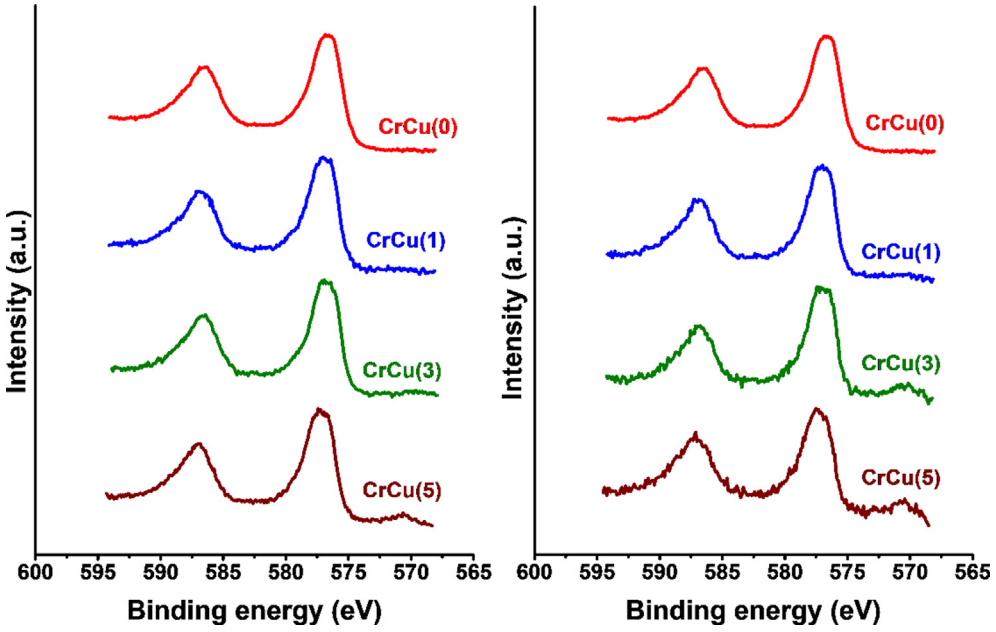

Fig. 9. Cr 2p region XPS spectra recorded after treatment of the catalysts under HTS conditions for 96 h at 2 bar (left) and 25 bar (right). Peaks at BE = ±570 eV corresponds to Cu LMM [50].

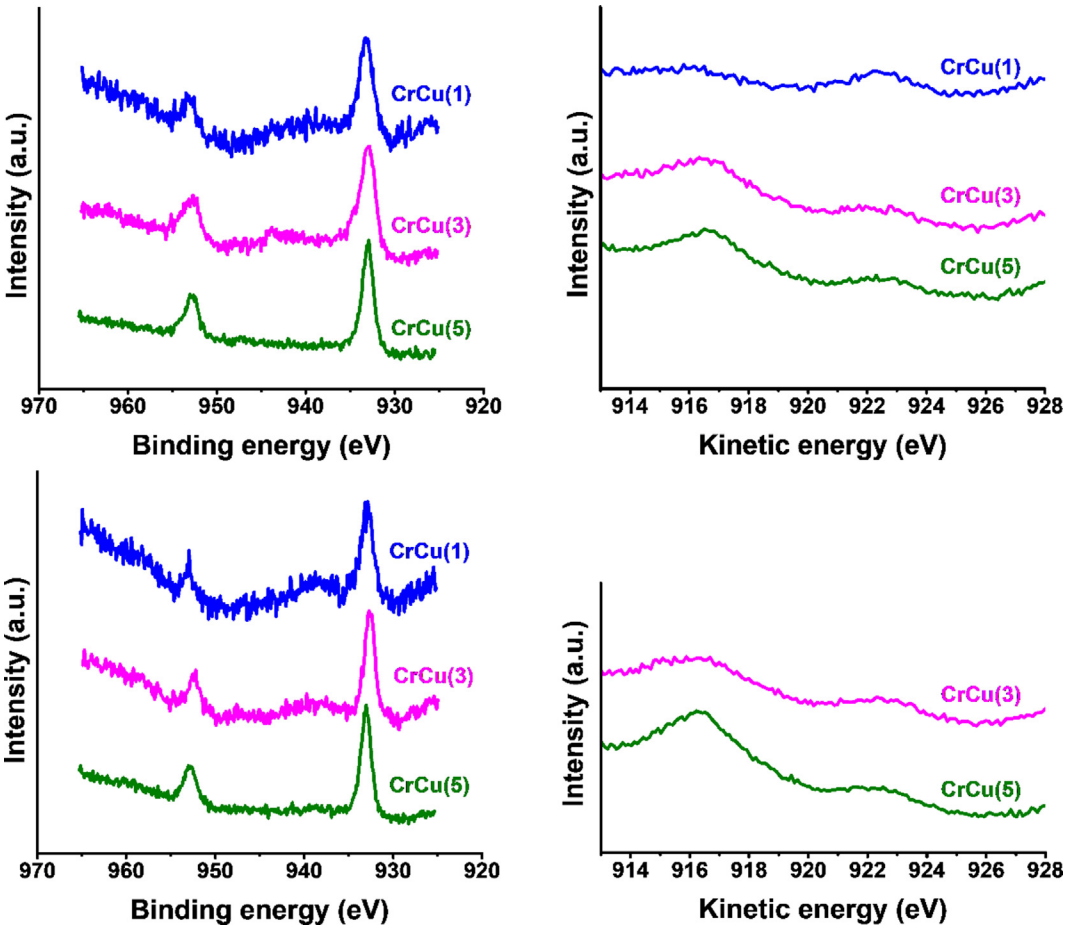

Fig. 10. XPS spectra Cu 2p and Cu LMM region after treatment under HTS conditions for 96 h at 2 bar (top) and 25 bar (bottom).

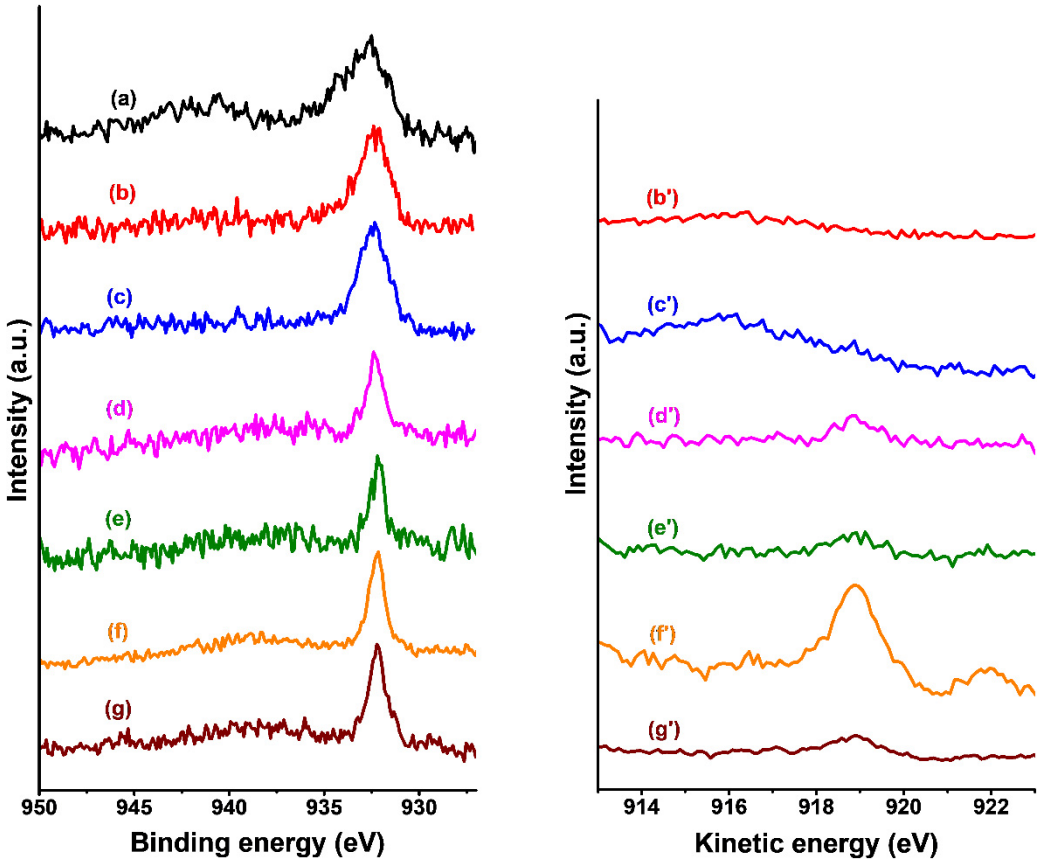

Fig. 11. Cu $2p_{3/2}$ region (a-g) and Cu LMM region (b'-g') of CrCu(5) during NAP-XPS measurements in a H_2O + CO (2:1) mixture [6]. Conditions: (a) fresh; (b, b') H_2O, 250 °C; (c, c') H_2O + CO, 250 °C; (d, d') H_2O + CO, 450 °C; (e, e') H_2O + CO, 250 °C; (f, f') H_2O, 250 °C o.n.; (g, g') O_2, RT.

conversion at ambient and industrially relevant pressure by acting as a chemical promoter, which results in the formation of new active surface sites. Increased pressure has no effect on the chromium- and copper-induced activity increase nor on the bulk structure of the catalyst.

Declaration of Competing Interest

The authors declare that they have no known competing financial interests or personal relationships that could have appeared to influence the work reported in this paper.

Acknowledgements

This publication is part of the project "Application of advanced combined in-situ Mössbauer/IR/GC characterisation under industrially relevant conditions to underpin and accelerate development of improved Fe-based catalysts" with project number 731.015.419 of the research programme LIFT and has received funding from the Dutch Research Council (NWO) and Johnson Matthey. The authors would like to thank Freddy Oropeza Palacio and Tiny Verhoeven for their help with XPS measurements, Valerii Muravev for his help with the NAP-XPS experiments, Arno van Hoof for TEM measurements, and Michel Steenvoorden for his help with the Mössbauer spectroscopy setup.

Appendix A. Supplementary data

Supplementary data to this article can be found online at https://doi.org/10.1016/j.jcat.2021.12.013.

References

[1] M. Zhu, I.E. Wachs, Iron-Based Catalysts for the High-Temperature Water-Gas Shift (HT-WGS) Reaction: A Review, ACS Catal. 6 (2) (2016) 722–732.
[2] D.-W. Lee, M.S. Lee, J.Y. Lee, S. Kim, H.-J. Eom, D.J. Moon, K.-Y. Lee, The review of Cr-free Fe-based catalysts for high-temperature water-gas shift reactions, Catal. Today 210 (2013) 2–9.
[3] IEA *The Future of Hydrogen*; https://www.iea.org/reports/the-future-of-hydrogen; 2019.
[4] D.S. Newsome, The Water-Gas Shift Reaction, Catal. Rev. Sci. Eng. 21 (2) (1980) 275–318.
[5] Martyn V. Twigg, Catalyst handbook, 2 ed., CRC Press, 1989.
[6] Minghui Zhu, Tulio C.R. Rocha, Thomas Lunkenbein, Axel Knop-Gericke, Robert Schlögl, Israel E. Wachs, Promotion Mechanisms of Iron Oxide-Based High Temperature Water-Gas Shift Catalysts by Chromium and Copper, ACS Catal. 6 (2016) 4455–4464.
[7] C. Ratnasamy, J.P. Wagner, Water Gas Shift Catalysis, Catalysis Rev. 51 (3) (2009) 325–440.
[8] C.J. Keturakis, Minghui Zhu, Emma K. Gibson, Marco Daturi, Franklin Tao, Anatoly I. Frenkel, Israel E. Wachs, Dynamics of CrO_3-Fe_2O_3 Catalysts during the High-Temperature Water-Gas Shift Reaction: Molecular Structures and Reactivity, ACS Catal. 6 (2016) 4786–4798.
[9] D. Damma, P.G. Smirniotis, Recent advances in iron-based high-temperature water-gas shift catalysis for hydrogen production, Curr. Opin. Chem. Eng. 21 (2018) 103–110.
[10] A. Khan, P.G. Smirniotis, Relationship between temperature-programmed reduction profile and activity of modified ferrite-based catalysts for WGS reaction, J. Mol. Catal. A: Chem. 280 (1–2) (2008) 43–51.
[11] C. Rhodes, G.J. Hutchings, A.M. Ward, Water-gas shift reaction: finding the mechanistic boundary, Catal. Today 23 (1995) 43–58.
[12] J.E. Kubsh, J.A. Dumesic, In situ gravimetric studies of the regenerative mechanism for water-gas shift over magnetite: Equilibrium and kinetic measurements in CO_2/CO and H_2O/H_2 gas mixtures, Am. Inst. Chem. Eng. 28 (5) (1982) 793–800.
[13] G.K. Boreskov, T.M. Yurieva, A.S. Sergeeva, Mechanism of the Conversion of Carbon Monoxide on Iron-Chromium Catalyst, Kinet. Catal. 11 (1970) 374–381.
[14] M. Robbins, G.K. Wertheim, R.C. Sherwood, D.N.E. Buchanan, Magnetic properties and site distributions in the system $FeCr_2O_4$-Fe_3O_4($Fe^{2+}Cr_{2-x}Fe^{3+}{}_xO_4$), J. Phys. Chem. Solids 32 (1971) 717–729.

[15] H.J. Levinstein, M. Robbins, C. Capio, A crystallographic study of the system $FeCr_2O_4$-Fe_3O_4($Fe^{2+}Fe^{3+x}Cr_{2-x}O_4$), Mat. Res. Bull. 7 (1972) 27–34.

[16] H. Topsøe, M. Boudart, Mossbauer spectroscopy of CO shift catalysts promoted with lead, J. Catal. 31 (1973) 346–359.

[17] S. Natesakhawat, X. Wang, L. Zhang, U.S. Ozkan, Development of chromium-free iron-based catalysts for high-temperature water-gas shift reaction, J. Mol. Catal. A: Chem. 260 (1–2) (2006) 82–94.

[18] M. Zhu, I.E. Wachs, A perspective on chromium-Free iron oxide-based catalysts for high temperature water-gas shift reaction, Catal. Today 311 (2018) 2–7.

[19] Michael Estrella, Laura Barrio, Gong Zhou, Xianqin Wang, Qi Wang, Wen Wen, Jonathan C. Hanson, Anatoly I. Frenkel, Jose A. Rodriguez, In Situ Characterization of $CuFe_2O_4$ and Cu/Fe_3O_4 Water-Gas Shift Catalysts, J. Phys. Chem. C 113 (2009) 14411–14417.

[20] A. Puig-Molina, F.M. Cano, T.V.W. Janssens, The Cu Promoter in an Iron−Chromium−Oxide Based Water−Gas Shift Catalyst under Industrial Conditions Studied by in-Situ XAFS, J. Phys. Chem. C 114 (36) (2010) 15410–15416.

[21] Minghui Zhu, Pengfei Tian, Ravi Kurtz, Thomas Lunkenbein, Jing Xu, Robert Schlogl, Israel E. Wachs, Yi-Fan Han, Strong Metal-Support Interactions between Copper and Iron Oxide during the High-Temperature Water-Gas Shift Reaction, Angew. Chem. 131 (2019) 9181–9185.

[22] Minghui Zhu, Pengfei Tian, Jiacheng Chen, Michael E. Ford, Jing Xu, Israel E. Wachs, Yi-Fan Han, Activation and deactivation of the commercial-type CuO–Cr_2O_3–Fe_2O_3 high temperature shift catalyst, AIChE J. (2020). https://doi.org/10.1002/aic.16846 66:e16846.

[23] C. Pellerin, S.M. Booker, Reflections on hexavalent chromium: health hazards of an industrial heavyweight, Environmental healts perspectives 108 (2000) A402–A407.

[24] F. Meshkani, M. Rezaei, Preparation of Mesoporous Chromium Promoted Magnetite Based Catalysts for High Temperature Water Gas Shift Reaction, Ind. Eng. Chem. Res. 54 (4) (2015) 1236–1242.

[25] Tiberiu Popa, Guoqing Xu, Thomas F. Barton, Morris D. Argyle, High temperature water gas shift catalysts with alumina, Appl. Catal. A: Gen. 379 (2010) 15–23.

[26] Emerentino Brazil Quadro, Maria de Lourdes Ribeiro Dias, Adelaide Maria Mendonça Amorim, Maria do Carmo Rangel, Chromium and Copper-Doped Magnetite Catalysts for the High Temperature Shift Reaction, J. Braz. Chem. Soc. 10 (1999) 51–59.

[27] M.A. Edwards, D.M. Whittle, C. Rhodes, A.M. Ward, D. Rohan, M.D. Shannon, G. J. Hutchings, C.J. Kiely, Microstructural studies of the copper promoted iron oxide/chromia water-gas shift catalyst, Phys. Chem. Chem. Phys. 4 (2002) 3902–3908.

[28] G.K. Reddy, P. Boolchand, P.G. Smirniotis, Unexpected Behavior of Copper in Modified Ferrites during High Temperature WGS Reaction-Aspects of Fe^{3+} –> Fe^{2+} Redox Chemistry from Mossbauer and XPS Studies, J. Phys. Chem. C 116 (2012) 11019–11031.

[29] V.P. Santos, T.A. Wezendonk, J.J.D. Jaén, A.I. Dugulan, M.A. Nasalevich, H.-U. Islam, A. Chojecki, S. Sartipi, X. Sun, A.A. Hakeem, A.C.J. Koeken, M. Ruitenbeek, T. Davidian, G.R. Meima, G. Sankar, F. Kapteijn, M. Makkee, J. Gascon, Metal organic framework-mediated synthesis of highly active and stable Fischer-Tropsch catalysts, Nat. Commun. 6 (1) (2015), https://doi.org/10.1038/ncomms7451.

[30] H. Topsøe, J.A. Dumesic, S. Mørup, Applications of Mössbauer Spectroscopy, Vol. II, Academic Press, New York, 1980.

[31] G.K. Reddy, S.J. Kim, J. Dong, P.G. Smirniotis, J.B. Jasinski, Long-term WGS stability of Fe/Ce and Fe/Ce/Cr catalysts at high and low steam to CO ratios-XPS and Mössbauer spectroscopic study, Appl. Catal. A 415-416 (2012) 101–110.

[32] M.I. Ariëns, V. Chlan, P. Novák, L.G.A. van de Water, A.I. Dugulan, E. Brück, E.J. M. Hensen, The role of chromium in iron-based high-temperature water-gas shift catalysts under industrial conditions, Appl. Catal. B 297 (2021) 120465, https://doi.org/10.1016/j.apcatb.2021.120465.

[33] Z. Klencsár, Mössbauer spectrum analysis by Evolution Algorithm, Nucl. Instrum. Methods Phys. Res., Sect. B 129 (4) (1997) 527–533.

[34] T. Yamashita, P. Hayes, Analysis of XPS spectra of Fe^{2+} and Fe^{3+} ions in oxide materials, Appl. Surf. Sci. 254 (8) (2008) 2441–2449.

[35] A. Parastaev, V. Muravev, E. Huertas Osta, A.J.F. van Hoof, T.F. Kimpel, N. Kosinov, E.J.M. Hensen, Boosting CO_2 hydrogenation via size-dependent metal–support interactions in cobalt/ceria-based catalysts, Nat. Catal. 3 (6) (2020) 526–533, https://doi.org/10.1038/s41929-020-0459-4.

[36] G.K. Reddy, P.G. Smirniotis, Effect of Copper as a Dopant on the Water Gas Shift Activity of Fe/Ce and Fe/Cr Modified Ferrites, Catal. Lett. 141 (2011) 27–32.

[37] M. Zhu, Ö. Yalçın, I.E. Wachs, Revealing structure-activity relationships in chromium free high temperature shift catalysts promoted by earth abundant elements, Appl. Catal. B 232 (2018) 205–212.

[38] G. Doppler, A.X. Trautwein, H.M. Ziethen, E. Ambach, R. Lehnert, M.J. Sprague, U. Gonser, Physical and Catalytic Properties of High-Temperature Water-Gas Shift Catalysts Based upon Iron-Chromium oxides, Appl. Catal. 40 (1988) 119–130.

[39] O. Ozdemir, D.J. Dunlop, T.S. Berquo, Morin transition in hematite: Size dependence and thermal hysteresis, Geochem. Geophys. Geosystems 9 (2008) 1–12.

[40] A. Khan, P. Chen, P. Boolchand, P.G. Smirniotis, Modified nano-crystalline ferrites for high-temperature WGS membrane reactor applications, J. Catal. 253 (2008) 91–104.

[41] R.M. Cornel, U. Schwertmann, Iron oxides—structure, properties, reactions, occurrences and uses, WILEY-VCH Verlag, Weinheim, Germany, 2003, pp. 155–156.

[42] Tahmin Lais, Liliana Lukashuk, Leon van de Water, Timothy I. Hyde, Matteo Aramini, Gopinathan Sankar, Elucidation of copper environment in a Cu–Cr–Fe oxide catalyst through in situ high-resolution XANES investigation, Phys. Chem. Chem. Phys. 23 (2021) 5888–5896.

[43] G.M. da Costa, C. Blanco-Andujar, E. De Grave, Q.A. Pankhurst, Magnetic Nanoparticles for in Vivo Use: A Critical Assessment of Their Composition, J. Phys. Chem. B 118 (40) (2014) 11738–11746.

[44] C.E. Johnson, J.A. Johnson, H.Y. Hah, M. Cole, S. Gray, V. Kolesnichenko, P. Kucheryavy, G. Goloverda, Mossbauer studies of stoichiometry of Fe_3O_4: characterization of nanoparticles for biomedical applications, Hyperfine Interact. 237 (2016) 1–10, 27.

[45] I.S. Lyubutin, C.R. Lin, Y.V. Korzhetskiy, T.V. Dmitrieva, R.K. Chiang, Mössbauer spectroscopy and magnetic properties of hematite/magnetite nanocomposites, J. Appl. Phys. 106 (3) (2009), https://doi.org/10.1063/1.3194316 034311.

[46] Z. Klencsár, A. Ábrahám, L. Szabó, E.G. Szabó, S. Stichleutner, E. Kuzmann, Z. Homonnay, G. Tolnai, Attila Ábrahám; László Szabó; Ervin Gy Szabó; Sándor Stichleutner; Ernõ Kuzmann; Zoltán Homonnay; Gyula Tolnai The effect of preparation conditions on magnetite nanoparticles obtained via chemical co-precipitation, Mater. Chem. Phys. 223 (2019) 122–132.

[47] M.d.C. Rangel, R.M. Sassaki, F. Galembeck, Renato Massami Sassaki; Fernando Galembeck Effect of chromium on magnetite formation, Catal. Lett. 33 (3-4) (1995) 237–254.

[48] M.F.F. Lelis, A.O. Porto, C.M. Goncalves, J.D. Fabris, Cation occupancy sites in synthetic Co-doped magnetites as determined with X-ray absorption (XAS) and Mossbauer spectroscopies, J. Magn. Magn. Mater. 278 (2004) 263–269.

[49] M.C. Biesinger, B.P. Payne, A.P. Grosvenor, L.W.M. Lau, A.R. Gerson, R.St.C. Smart, Resolving surface chemical states in XPS analysis of first row transition metals, oxides and hydroxides: Cr, Mn, Fe, Co and Ni, Appl. Surf. Sci. 257 (2011) 2717–2730.

[50] L.i. Zhang, L. Han, G. Zhao, R. Chai, Q. Zhang, Y.e. Liu, Y. Lu, Structured Pd–Au/Cu-fiber catalyst for gas-phase hydrogenolysis of dimethyl oxalate to ethylene glycol, Chem. Commun. 51 (52) (2015) 10547–10550.

[51] Y. Gao, E.J.M. Hensen, Highly active and stable spinel-oxide supported gold catalyst for gas-phaseselective aerobic oxidation of cyclohexanol to cyclohexanone, Catal. Commun. 117 (2018) 53–56.

[52] I. Platzman, R. Brener, H. Haick, R. Tannenbaum, Oxidation of Polycrystalline Copper Thin Films at Ambient Conditions, J. Phys. Chem. C 112 (4) (2008) 1101–1108.

[53] T. Shishido, M. Yamamoto, I. Atake, D. Li, Y. Tian, H. Morioka, M. Honda, T. Sano, K. Takehira, Cu/Zn-based catalysts improved by adding magnesium for water–gas shift reaction, J. Mol. Catal. A: Chem. 253 (1-2) (2006) 270–278.

[54] L. Yuan, Q. Yin, Y. Wang, G. Zhou, CuO reduction induced formation of CuO/Cu_2O hybrid oxides, Chem. Phys. Lett. 590 (2013) 92–96.